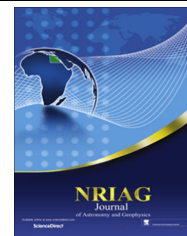National Research Institute of Astronomy and Geophysics

NRIAG Journal of Astronomy and Geophysics

www.elsevier.com/locate/nrjag

Magnetic and gravity data analysis of Rahat Volcanic Field, El-Madinah city, Saudi Arabia

Essam Aboud [a,*], Nabil El-Masry [a], Atef Qaddah [a], Faisal Alqahtani [b], Mohammed R.H. Moufti [a]

[a] *Geohazards Research Center, King Abdulaziz University, P.O. Box 80206, Jeddah 21589, Saudi Arabia*
[b] *Faculty of Earth Science, King Abdulaziz University, P.O. Box 80206, Jeddah 21589, Saudi Arabia*

Abstract   The Rahat volcanic field represents one of the widely distributed Cenozoic volcanic fields across the western regions of the Arabian Peninsula. Its human significance stems from the fact that its northern fringes, where the historical eruption of 1256 A.D. took place, are very close to the holy city of Al-Madinah Al-Monawarah.

In the present work, we analyzed aeromagnetic data from the northern part of Rahat volcanic field as well as carried out a ground gravity survey. A joint interpretation and inversion of gravity and magnetic data were used to estimate the thickness of the lava flows, delineate the subsurface structures of the study area, and estimate the depth to basement using various geophysical methods, such as Tilt Derivative, Euler Deconvolution and 2D modeling inversion.

Results indicated that the thickness of the lava flows in the study area ranges between 100 m (above Sea Level) at the eastern and western boundaries of Rahat Volcanic field and getting deeper at the middle as 300–500 m. It also showed that, major structural trend is in the NW direction (Red Sea trend) with some minor trends in EW direction.

© 2015 Production and hosting by Elsevier B.V. on behalf of National Research Institute of Astronomy and Geophysics.

1. Introduction

Harrat Rahat (Harrat = Volcanic field) is one of the Cenozoic lava fields in Saudi Arabia. Volcanic field in Saudi Arabia extends across the western regions of the Arabian Peninsula from Yemen in the south to the Levant in the north. They markedly define different phases of magmatic activity that took place during the 30 million years history of the Red Sea–Gulf of Aden rift system (Camp et al., 1987; Camp and Roobol, 1989, 1991; Bosworth et al., 2005). The Rahat Volcanic Field (RVF) occupies a 50 km wide plateau that

* Corresponding author at: National Research Institute of Astronomy and Geophysics, NRIAG, Cairo, Egypt.
  E-mail address: eaboudishish@kau.edu.sa (E. Aboud).

extends from north to south for almost 300 km between the Hejaz coastal range on the west and the high plains of Najd on the east (Durozoy, 1970; Berthier et al., 1981) as shown in Fig. 1. It has an approximate volume of 2000 km^3 (Camp et al., 1987; Camp and Roobol, 1989, 1991) and an estimated average thickness of about 150 m south of latitude 24° N (Blank and Sadek, 1983). The most recent eruption of 1256 AD, which lasted for 52 days, extruded 0.5 km^3 of alkali-olivine basalt from a 2.25 km long fissure and produced 6 scoria cones and a 23 km-long lava flow that came to within 8 km from Al-Madinah city (Camp et al., 1987, 1989; Ambraseys et al., 1994).

Two major hazard events were documented and located within the study area; eruption of 1256 AD and the earthquake swarm in 1999 (El Difrawy et al., 2013). In the current study, we used gravity and magnetic data to evaluate the above mentioned hazards.

The objectives of the current work are to image the subsurface structure, estimate the average thickness of the overlying Cenozoic lava flows, and estimate the depth to the basement underneath the lava flows. Therefore, a ground gravity survey was carried out in the northern part of RVF using a CG5 gravimeter and a differential GPS instrument. Gravity data were used in parallel with the available aeromagnetic data over RVF and the surrounding Precambrian Arabian shield reported by the Bureau de Recherches Geologiques et Minieres (BRGM) and the Saudi Geological Survey (SGS), (BRGM, 1966.

In that regard, we used Euler deconvolution method to estimate the depth to the basement rocks from magnetic data, The Tilt Derivative (TDR) method to trace the major lineation in the area, and finally, 2D joint inversion of gravity and magnetic data to map the lava flows and estimate its thickness.

2. Geological setting

The northern terrains of RVF (Fig. 1), referred to as Harrat Al-Madinah (Moufti, 1985), are largely constructed of monogenetic, Strombolian-style basaltic volcanoes and basaltic lava flows, which extruded onto the Precambrian basement rocks of the Arabian Shield through NNW-trending *en echelon*-vent zones (Moufti et al., 2010). The basalts range from olivine transitional basalt and alkali olivine basalt to hawaiite, whereas the associated evolved rocks of mugearite, benmoreite, and trachyte occur mainly as domes and tuff cones as well as lava flows (Moufti et al., 2010, 2012). Harrat Al-Madinah basalts were further divided into the lower Madinah basalt and the upper Madinah basalt (Camp et al., 1987; Camp and Roobol, 1989, 1991). The upper Madinah basalts comprised three flow units, namely Qm1 (~1.7–1.2 Ma), Qm2 (~1.2–0.9 Ma), and Qm3 (~0.9–0.6 Ma), whereas the upper Madinah basalt included four flow units, namely Qm4 (~0.6–0.3 Ma), Qm5 (~0.3 Ma–4500 BP), Qm6 (~4500–1500 BP), and Qm7 (~1500 BP –1256 AD, Fig. 2), (Camp et al., 1987; Camp and Roobol, 1989, 1991).
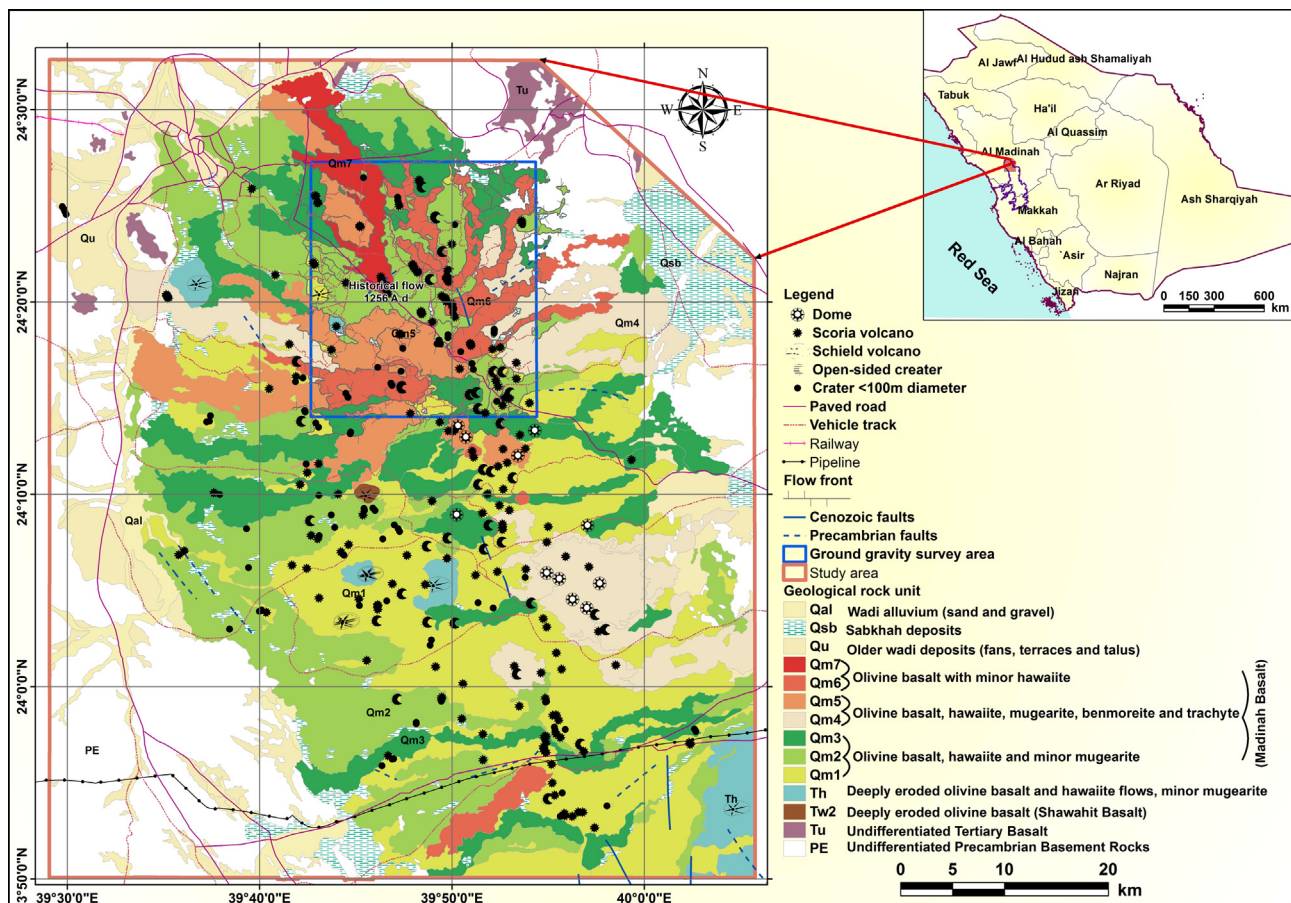

Figure 1 Geologic map of northern Rahat volcanic field (modified after Camp and Roobol, 1991).

The alignment of volcanic cones along right-stepping *en echelon* structures within the axial zone of RVF, in general, and Harrat Al-Madinah, in particular, was contributed to a left-lateral N–S shear originated by tension stresses of NE and ENE directions (Moufti et al., 2010). These stresses could have also caused the formation of a NNW-trending major graben in the Precambrian basement and the preferred alignment of the 501 volcanic cones of Harrat Al-Madinah along the NW–SE and N–S trends of the Red Sea rift and the left-lateral shear, respectively (Moufti et al., 2010).

3. Aeromagnetic data

Several aeromagnetic surveys were carried out between 1962 and 1983 by commercial companies (e.g. ARGAS) under the auspices of the Ministry of Petroleum and Mineral Resources of the Kingdom of Saudi Arabia, and supervised by BRGM and USGS. The surveys were conducted over individual blocks. They had ground clearances of 150, 300, or 500 m and a line spacing of about 800 m. The 1962 and 1965 to 1967 surveys supervised by BRGM covered the entire Arabian Shield, and were flown using fluxgate Gulf Mark III
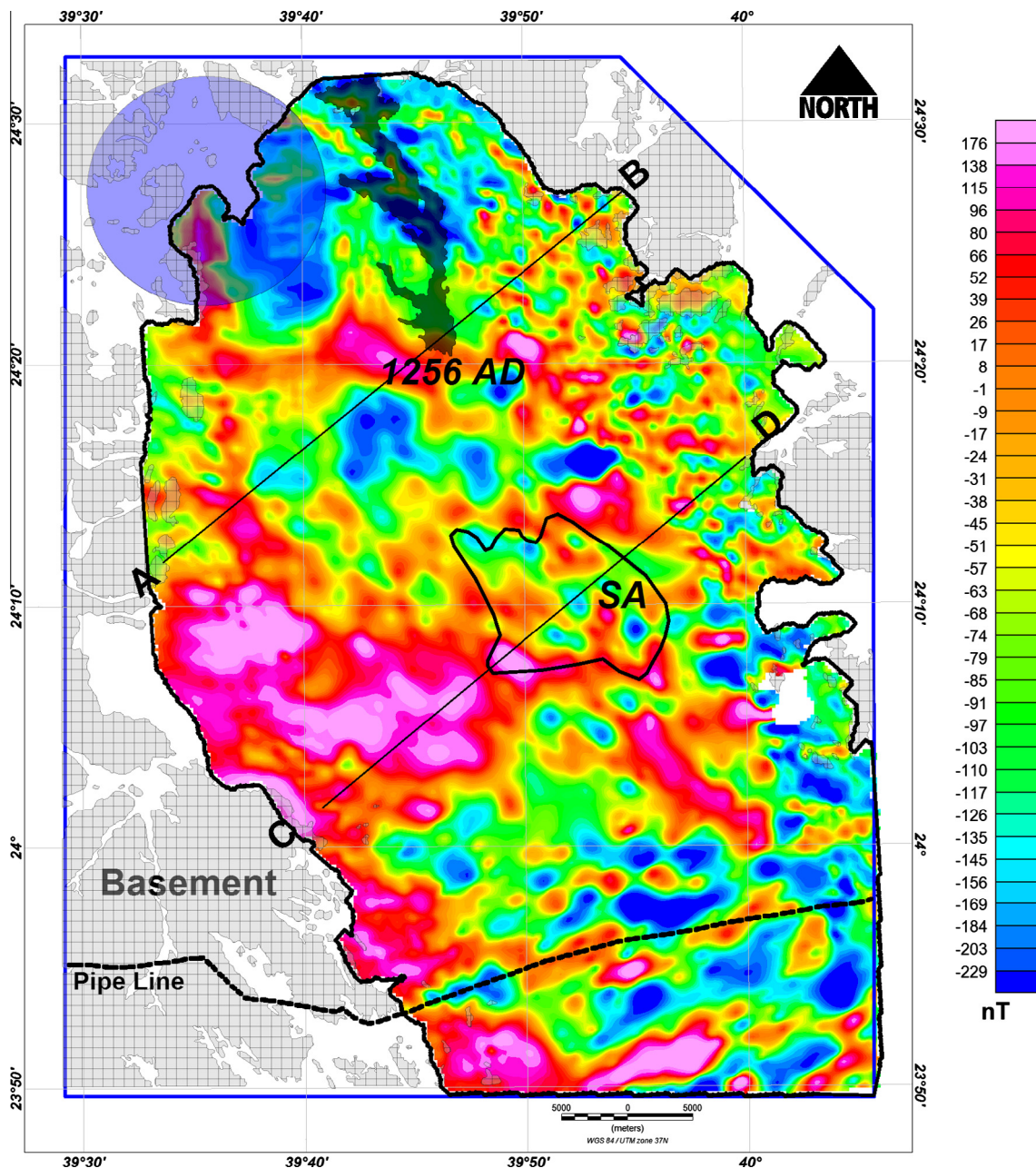

Figure 2 Shows the total intensity magnetic map of RVF. Gray hachure indicates the Precambrian exposed basement rocks on the surface. Dashed black line represents the Pipeline. SA = seismic swarm area (El Difrawy et al., 2013). The 1256 AD shows the location of historical eruption. AB and CD show the location of the modeling profiles. Transparency circle = Madinah City.

magnetometers with analog recording. In addition, five general and several less-extensive surveys, were carried out over targets of economic interest using (e.g. Rahat Volcanic Field) a CSF cesium-vapor magnetometer in 1976 and 1981, and a Geometrics G813 proton-precession magnetometer in 1983, both with digital recording. Fig. 2 shows the total intensity magnetic map of the study area.

Blank and Sadek (1983) use the spectral analysis technique to estimate the depth to the basement surface from aeromagnetic data south of Pipeline (Fig. 2) and concluded that maximum thickness estimated for the lava flow section is 380 m and the main is about 150 m.

Aeromagnetic data of RVF (north of latitude 24°) are displayed in Fig. 2 and indicated that, high and low magnetic anomalies are easily observed on the map reflecting the locations of shallow and deep basement rocks, respectively. It should be stated that, surface lava flows have magnetic contents a little similar to basement rocks that make it difficult to map the lava flow from magnetic data. The maximum and minimum magnetic anomaly values are 176 and −228 nT, respectively.

4. Gravity survey

Three field surveys were conducted during November 2011, January 2012, and March 2012 using a Scintrex Autograv CG5 gravity meter that has a resolution of 0.001 mGal.
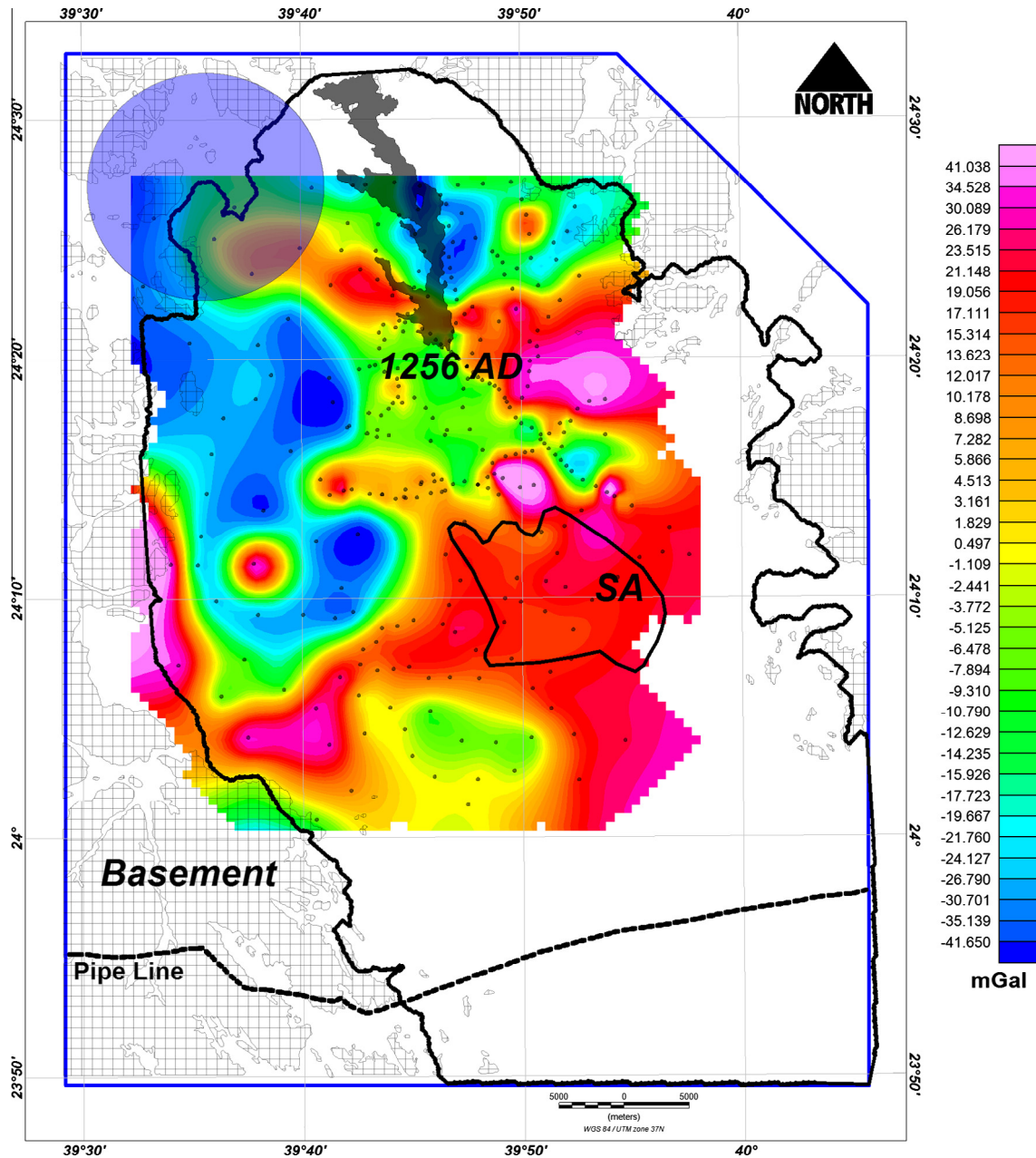

Figure 3 Shows the residual gravity anomaly map of the surveyed area. Black dots show the location of gravity station. SA = seismic swarm area (El Difrawy et al., 2013). The 1256 AD shows the location of historical eruption. AB and CD show the location of the modeling profiles. Transparency circle = Madinah City.

Gravity data points were sparse in areas where sharp lava flows were inaccessible. In other places, the survey was carried out by foot over broken terrain, reducing repeat/delay base station measurements. This is the most probable cause for the large closure errors (Zurek et al., 2012). However, the historical eruption (1256 AD) and swarm areas of the RFV were well covered. Gravity station intervals were between 300 and 1500 due to the available tracks and a little hard terrain.

To get high accuracy for the vertical and horizontal positions for each gravity station, a kinematic GPS survey was conducted using a continuous GPS station (base station) for 1s sampling interval and rover system from Leica system. Postprocessing of the data provides vertical accuracy on the

order of few centimeters. Finally, we had collected 293 gravity stations covering an area of 40 * 50 km (Fig. 3).

Once gravity data were corrected for terrain (using an average density of 2.67 gm/cm^3 as deduced from the surrounding volcanic rocks) and free-air effects, Bouguer anomaly map will be ready for interpretation. These data sets, contain contributions from both regional and local density anomalies. To obtain a residual Bouguer anomaly map highlighting only local density variations requires removal of the regional gravitational field (Nettleton, 1940). There are many different techniques to accomplish this; including fitting a surface to a dense basement or taking the second derivative of the data to enhance near-surface effects (e.g. Gupta and Ramani, 1982).
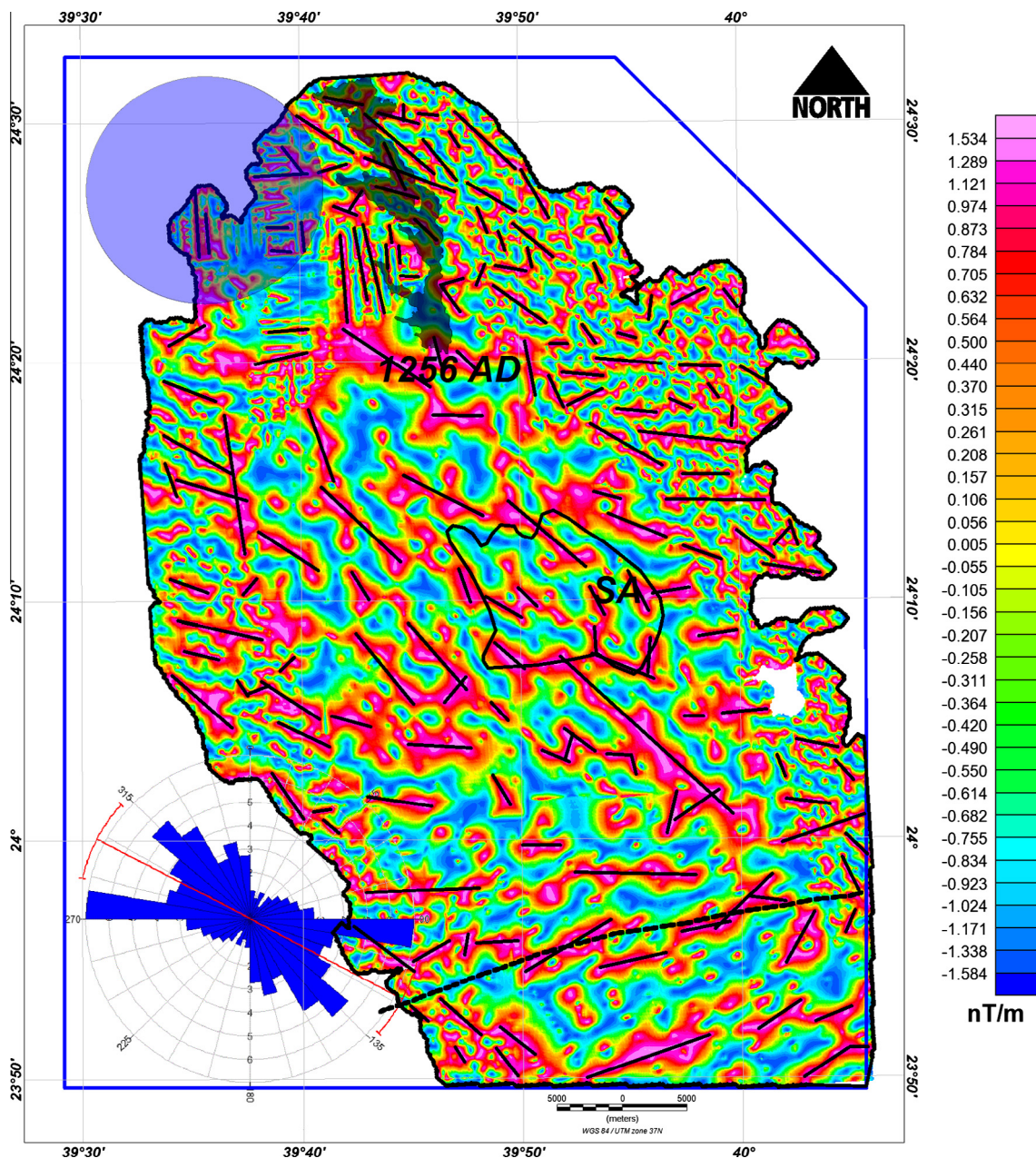

Figure 4 Shows the results of TDR method. Black straight lines indicate the location of contacts/faults/lineation. Rose diagram shows the main major trend of the faults in NW direction. SA = seismic swarm area (El Difrawy et al., 2013). The 1256 AD shows the location of historical eruption. Transparency circle = Madinah City.

In our case, we removed the regional gravity effect using a third order trend from a grid by least square fitting to all the values in the grid. The residual anomaly (Fig. 3) map shows that, low negative anomalies values (−2 to −40 mGal) covered the north western part (blue color in Fig. 3) where the high values (3–41 mGal) are located on the eastern part of the area (pink color in Fig. 3). The negative gravity signs indicate that the outcrops are formed by explosive activity, where surficial material has a low density (Malahoff, 1969).

5. Applications and results

Potential field data, either gravity or magnetic, incorporate ample information about the subsurface structures which makes it rather difficult to interpret their maps from the first glimpse. Therefore, filters are needed to enhance and/or sharpen anomaly edges or contacts and to remove the noise from the data. In that regard, some filters were applied to the aeromagnetic data of RVF to delineate its subsurface structures and to estimate the depth to the Precambrian basement. Gravity and magnetic data were subsequently used to produce 2D models for the subsurface structures.

5.1. Tilt derivative (TDR) filter

Tilt derivative (TDR) filter is usually used to detect the geological edges or contacts, which may represent faults, from magnetic data. The TDR and its total horizontal derivative are useful tools for mapping shallow basement structures. This filter is calculated by dividing the vertical derivative (VDR) component by the total horizontal derivative (THDR) of the magnetic field (Verduzco, 2004), where

$$TDR = \arctan(VDR/THDR) \qquad (1)$$

The ultimate advantage of the TDR filter is that its zero contour line value is on or close to a fault/contact/lineation location. TDR technique was applied to aeromagnetic data directly and the results were plotted as a grid image as shown in Fig. 4. Several magnetic linear anomalies can be recognized trending in a northwest direction, in the northern part of the surveyed area, whereas we see east west trends at the southern part of the study area. These linear anomalies represent subsurface faults or contacts in the study area. It is clear that, the study area was dissected by various faults trending in NW–NNW, direction parallel to the Red Sea trend. The Rose diagram shows (Fig. 4) the major and minor trend based on TDR analysis. Table 1 shows the Rose diagram statistics summary.

5.2. Depth to basement

Several methods, such as Euler deconvolution, analytic signal, and Werner deconvolution, can be used to estimate the depth to basement on a profile or grid from potential field data. In the present work, Euler deconvolution was used to map the basement from magnetic data. Euler deconvolution has come into wide use for automatic estimates of field source location and depth (Bournas et al., 2003; Shepherd et al., 2006; Chennouf et al., 2007; Li et al., 2008). This method was established by Thompson (1982) and has been applied essentially to real magnetic data along profiles. Reid et al. (1990) followed

Table 1 Rose diagram statistics summary.

Calculation method	Length
Class interval	10°
Population	165
Total length of all lineations	1192708.51
Maximum Bin Population	23
Mean Bin population	9.17
Standard deviation of Bin population	5.53
Maximum Bin Length (%)	85
Mean Bin Length (%)	33
Standard deviation for Bin length (%)	2.02
Vector mean	117
	297
Confidence interval	13.9
R-mag	0.42

up a suggestion in Thompson's paper and developed the equivalent grid method.

The 3-D equation of Euler deconvolution given by Reid et al. (1990) is

$$(x - x_0)\frac{\partial M}{\partial x} + (y - y_0)\frac{\partial M}{\partial y} + (z - z_0)\frac{\partial M}{\partial z} = n(b - M) \qquad (2)$$

where (x_o, y_o, z_o) are the positions of a source in which magnetic anomaly is detected at (x, y, z), b is the regional value of the magnetic (background) and n is the structural index (SI), which can be defined as the rate of attenuation of the anomaly with distance. The SI must be chosen according to a prior knowledge of the source geometry. For example, in the magnetic case, SI = 1 for dike, SI = 2 for sill, SI = 0 for contact (FitzGerald et al., 2004). The two horizontal gradients $(\partial M/\partial x, \partial M/\partial y)$ and vertical $(\partial M/\partial z)$ derivatives are used to apply the Euler method.

By considering four or more neighboring observations at a time (an operating window), source location (x_o, y_o, z_o) and b can be computed by solving a linear system of equations generated from Eq. (1). Then, by moving the operating window from one location to the next over the anomaly, multiple solutions for the same source are obtained.

In our study, the Euler method has been applied to the aeromagnetic data using a SI = 0 and moving window of 0.5 km, and the grid cell size of the magnetic data was 250 m. We have assigned several structural indices values and found that an SI of zero gives good clustering solutions. Reid et al. (1990) and Reid et al. (2003) presented a structural index equal to zero for delineating faults. Results of the Euler deconvolution of magnetic data are shown in Fig. 5. In that regard, we plotted Euler solution in different way where instead of Symbols location, we used grid in order to extract modeling profile data from grid. It can be stated that, depths ranged from 105 m (above S.L.) at the eastern and western borders of the RVF where it gets deeper (> 280 m) at the center of the study area. The pink color in Fig. 5 indicates the deep basement surface, which is located at the main central part of the volcanic field.

5.3. 2D modeling technique

In order to take advantage of the joint inversion technique, magnetic and gravity data were used to estimate the lava flow
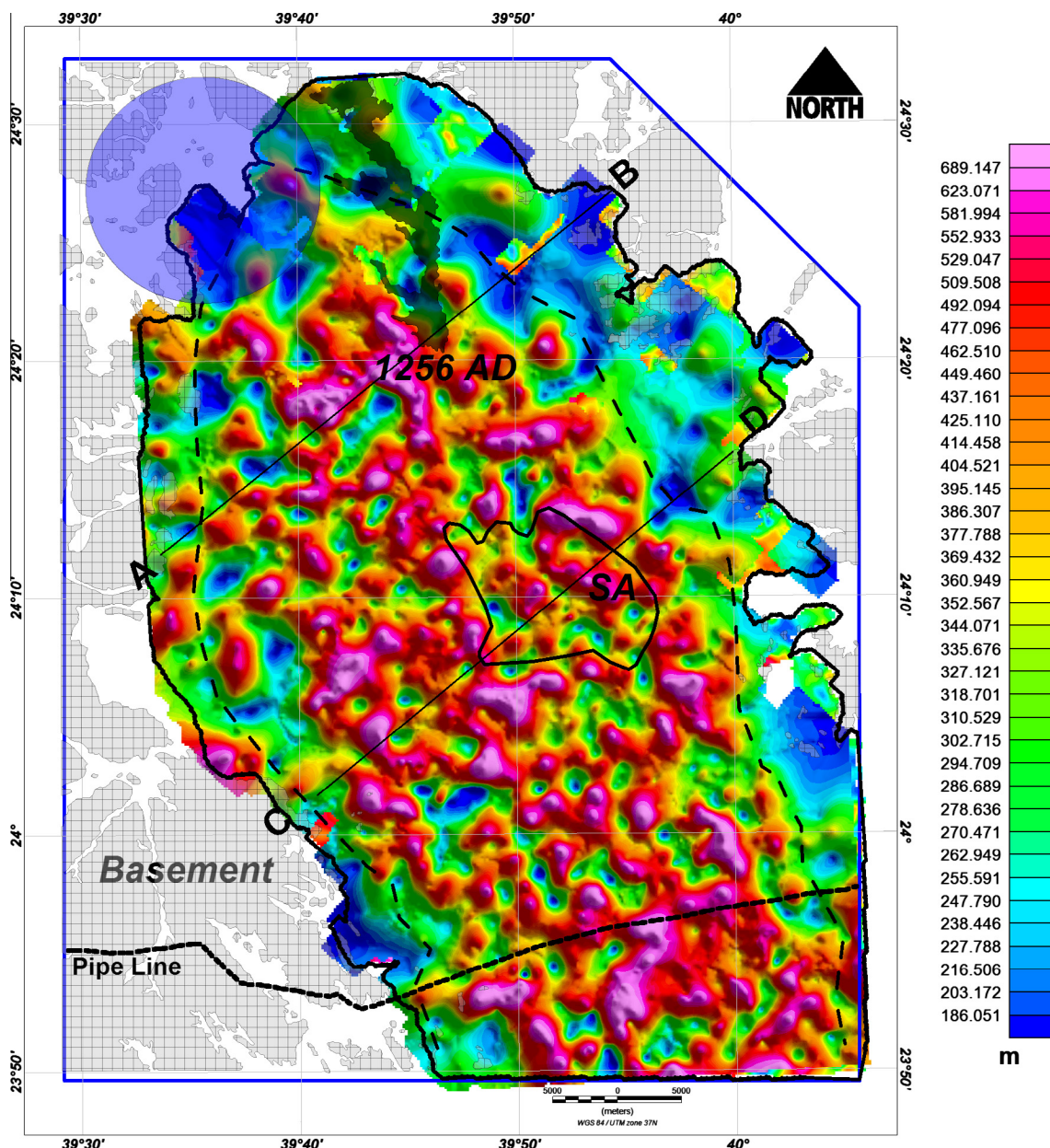
Figure 5 Shows Euler deconvolution map as a grid where pink color shows the location of the deep basement surface which reflects a graben structure trending in NW direction. Dashed line shows the basin border. SA = seismic swarm area (El Difrawy et al., 2013). The 1256 AD shows the location of historical eruption. AB and CD profiles show the location of the modeling profiles. Transparency circle = Madinah City.

thickness. GM-SYS 2D package from Oasis Montaj was used as a program for calculating the gravity and magnetic response from a geological cross-section model. GM-SYS provides easy-to-use interface for interactively creating and manipulating models to fit observed gravity and/or magnetic data. Rapid calculation of the gravity and magnetic response from 2D and $2\frac{3}{4}$ D models speed the interpretation process and allow us to quickly test alternative solutions. 2D models assume the earth is two-dimensional, i.e. it changes with depth (the Z direction) and in the direction of the profile (X direction; perpendicular to strike). 2D models do not change in

the strike direction (Y direction). 2D blocks and surfaces are presumed to extend to infinity in the strike direction.

Two profiles (AB and CD) were selected as shown in Fig. 2 to apply the modeling inversion. Gravity and magnetic models are not unique solutions (i.e., several Earth models can produce the same gravity and/or magnetic response). Furthermore, many solutions may not be geologically realistic. It is the task of the interpreter to evaluate the "geologic reasonableness" of any model. In order to avoid this trick and minimize the error, basement surface (horizon) was exported from Euler results and imported into the inversion. Then slight
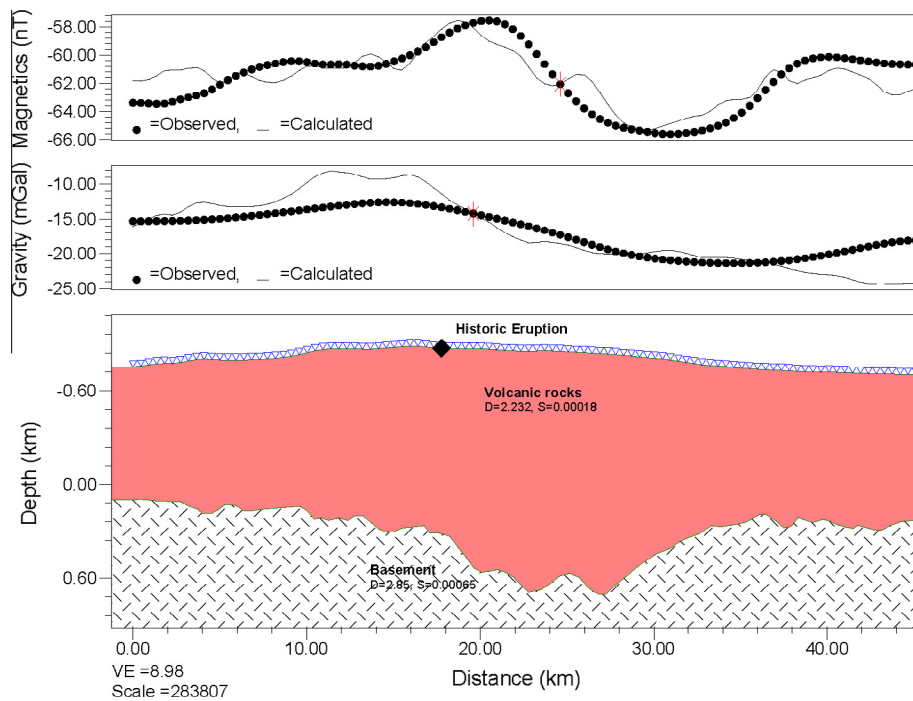
Figure 6   Shows the AB profile modeling. Basement surface was exposed on 0 m depth from Sea level and overlain by lava flows.
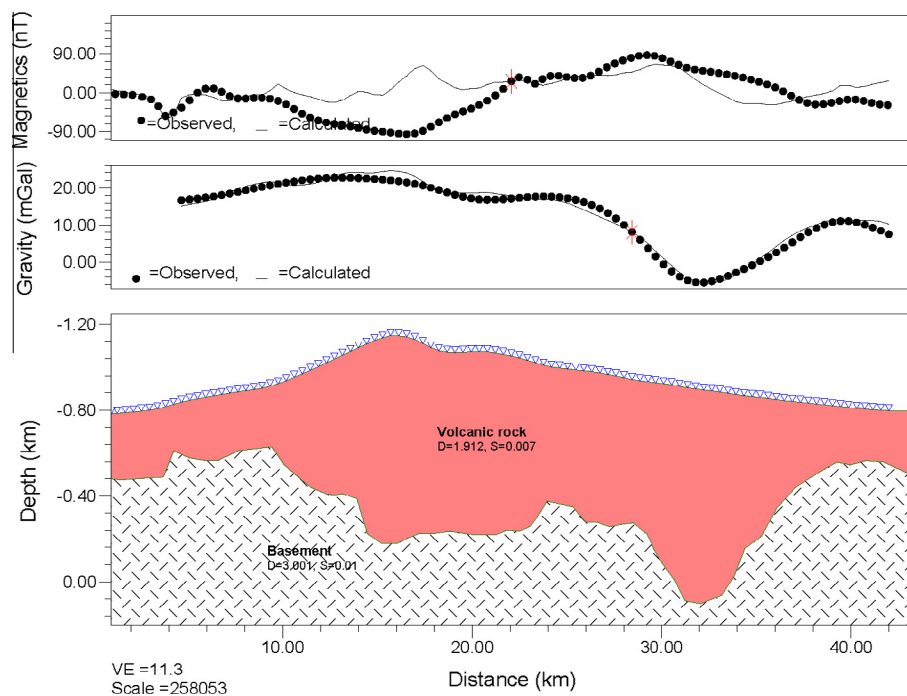

Figure 7   Shows the CD profile for modeling. Basement surface was exposed on 0–250 m depth from Sea level.

changes in the depth horizon were made to get the best fit between the observed and the calculated potential field data as shown in Figs. 6 and 7. DEM data were used to incorporate the topography into the inversion. Figs. 6 and 7 show the inversion results of AB profile and indicated that, the high thickness lava flow was located at the center of RVF underneath the historic eruption 1256 AD supporting the idea of existence of basin under the RVF.

6. Discussion and conclusions

Aeromagnetic and gravity data for the Rahat volcanic field were integrated to delineate the subsurface structures of the northern part of area. Results indicated that Rahat volcanic field superimposes a major NW-trending graben system (70 km long by 30 km wide) that runs parallel to the Red Sea, which could explain that these volcanic fields were formed due to the extension of the Red Sea rift. Dashed line in Fig. 5 shows the main borders of the graben system including the volcanic cones of the study area.

Different sets of faults, particularly the NW and NNW trending, were formed during the 30 M history of the Red Sea rift. Many of these faults, however, are not clearly visible on the ground surface as the Precambrian basement is covered by a relatively thick succession of Cenozoic lava flows. Therefore, the use of the TDR method was necessary to disclose the distribution and density of the whole-range of faults cutting across the study area, including concealed-subsurface structures. TDR method identified 165 faults in an area of 3000 km^2. The faults have a total length of 1000 km. The trend of their mean vector is 315°.

Results showed that potential field methods were also successful in imaging subsurface structures and in estimating the depth to the Precambrian basement of the northern part of Rahat volcanic field. Therefore, we recommend that TDR method and Euler deconvolution should be used on the potential field data covering the entire 300 km long Rahat volcanic field.

Additionally, thicknesses of lava flows were determined by 2D inversion showing lava flow thickness is increased at the center and decreased at east and western part of the study area.

Acknowledgments

References

ARGAS, 1976. USGS-BRGM airborne magnetometer survey, Harrat Rahat. Arabian Geophysical and Surveying Company (ARGAS) Report, p. 22.

Berthier, F., Demange, J., Iundt, F., Verzier, P., 1981. Geothermal resources of the Kingdom of Saudi Arabia. Saudi Arabian Deputy Ministry for Mineral Resources Open-File Report BRGM-OF-01-24, p. 116.

Blank, H.R., Sadek, H.S., 1983. Spectral analysis of the 1976 aeromagnetic survey of Harrat Rahat, Kingdom of Saudi Arabia. Saudi Arabian Deputy Ministry for Mineral Resources Open-File Report USGS-OF-03-67, p. 29.

Bosworth, W., Huchon, P., McClay, K., 2005. The Red Sea and Gulf of Aden Basins. J. Afr. Earth Sc. 43, 334–378.

Bournas, N., Galdeano, A., Hamoudi, M., Baker, H., 2003. Interpretation of the aeromagnetic map of Eastern Hoggar (Algeria) using the Euler deconvolution, analytic signal and local wavenumber methods. J. Afr. Earth Sc. 37, 191–205.

BRGM, 1966. Aeromagnetic and scintillometric survey flight operations, final report. Bureau de Recherches Geologiques et Minieres, Saudi Arabian Mission, Final Report SG-JED-66-B-1, p. 11.

Camp, V.E., Roobol, M.J., 1989. The Arabian continental alkali basalt province: Part I, Evolution of Harrat Rahat, Kingdom of Saudi Arabia. Geol. Soc. Am. Bull. 101, 71–95.

Camp, V.E., Roobol, M.J., 1991. Geologic map of the Cenozoic lava field of Harrat Rahat, Kingdom of Saudi Arabia. Saudi Arabian Directorate General of Mineral Resources, Geoscience Map GM-123, scale 1:250,000.

Camp, V.E., Hooper, P.R., Roobol, M.J., White, D.L., 1987. The Madinah eruption, Saudi Arabia: magma mixing and simultaneous extrusion of three basaltic chemical types. Bull. Volcanol. 49, 489–508.

Camp, V.E., Hooper, P.R., Roobol, M.J., White, D.L., 1989. The Madinah historical eruption: magma mixing and simultaneous extrusion of three basaltic chemical types. Saudi Arabian Directorate General of Mineral Resources, Open File Report DGMR-OF-06-32, p. 52.

Chennouf, T. et al, 2007. Major structural trends in northeastern Morocco: the contribution of gravimetry. C.R. Geosci. 339, 383–395.

Durozoy, G., 1970. Groundwater geology of the basalt on the Harrat Rahat plateau. Bureau de Recherches Geologicques et Minieres (BRGM), Saudi Arabian Mission, Open-File Report, 70 JED 24, p. 31.

El Difrawy, M.A., Runge, M.G., Moufti, M.R., Cronin, S.J., Bebbington, M., 2013. A first hazard analysis of the Quaternary Harrat Al-Madinah volcanic field, Saudi Arabia. J. Volcanol. Geotherm. Res. 267, 39–46.

FitzGerald, D., Reid, A., McInerney, P., 2004. New discrimination techniques for Euler Deconvolution. Comput. Geosci. 30, 461–469.

Gupta, V.K., Ramani, N., 1982. Optimum second vertical derivatives in geologic mapping and mineral exploration. Geophysics 47, 1706–1715.

Li, C.-F. et al, 2008. Late Mesozoic tectonic structure and evolution along the present-day northeastern South China Sea continental margin. J. Asian Earth Sci. 31, 546–561.

Malahoff, A., 1969. Gravity anomalies over volcanic regions. Geophys. Monogr. Ser. 13, 364–379.

Moufti, M.R., 1985. The geology of Harrat Al Madinah volcanic field, Harrat Rahat, Saudi Arabia. Unpublished Ph.D. Thesis, University of Lancaster, UK, p. 476.

Moufti, M.R., El-Difrawy, M.A.-M., Soliman, M.A.-W., El-Moghazi, A.-K.M., Matsah, M.I., 2010. Assessing volcanic hazards of a Quaternary lava field in the Kingdom of Saudi Arabia. King Abdulaziz City for Science and Technology (KACST), Final Report ARP-26-79.

Moufti, M.R., Moghazi, A.M., Ali, K.A., 2012. Geochemistry and Sr–Nd–Pb isotopic composition of the Harrat Al-Madinah Volcanic Field, Saudi Arabia. Gondwana Res. 21, 670–689.

Nettleton, L.L., 1940. Geophysical Prospecting for Oil. McGraw-Hill, New York.

Reid, A.B. et al, 1990. Magnetic interpretation in three dimensions using Euler Deconvolution. Geophysics 55, 80–91.

Reid, A.B., FitzGerald, D., McInerney, P., 2003. Euler Deconvolution of gravity data. Society of Exploration Geophysicists (SEG). Annual Meeting, pp. 580–583.

Shepherd, T., Bamber, J.L., Ferraccioli, F., 2006. Subglacial geology in Coats Land, East Antarctica, revealed by airborne magnetics and radar sounding. Earth Planet. Sci. Lett. 244, 323–335.

Verduzco, B., 2004. New insights into magnetic derivatives for structural mapping. Lead. Edge 23, 116–119.

Zurek, J.M., Williams-Jones, G., Johnson, D., Eggers, A., 2012. Constraining volcanic inflation at Three Sisters Volcanic Field in Oregon, U.S.A., through microgravity and deformation modeling. Geochem. Geophys. Geosyst. 10, Q10013.